Scripta Materialia 178 (2020) 29–33

Contents lists available at ScienceDirect

Scripta Materialia

journal homepage: www.elsevier.com/locate/scriptamat

Stabilization of ultrafine-grained microstructure in high-purity copper by gas-filled pores produced by severe plastic deformation

Yuanshen Qi[a,*], Anna Kosinova[a], Askar R. Kilmametov[b,c], Boris B. Straumal[b,c,d], Eugen Rabkin[a,*]

[a] Department of Materials Science and Engineering, Technion – Israel Institute of Technology, 3200003 Haifa, Israel
[b] Karlsruhe Institute of Technology, Institute of Nanotechnology, Eggenstein-Leopoldshafen 76344, Germany
[c] Institute of Solid State Physics and Chernogolovka Scientific Center, Russian Academy of Sciences, Chernogolovka 142432, Russia
[d] National University of Science and Technology «MISIS», Moscow 119049, Russia

ARTICLE INFO

Article history:
Received 15 September 2019
Revised 24 October 2019
Accepted 28 October 2019

Keywords:
Grain boundary migration
Thermal stability
High-pressure torsion
Copper
Electron energy loss spectroscopy (EELS)

ABSTRACT

We observed very high thermal stability (after annealing at 600 °C for 1 h) of the near-surface layers of ultrafine grains in the 99.9995 wt% (5N5) purity Cu processed by high-pressure torsion. We attributed this extraordinary thermal stability of ultrafine-grained microstructure to the nitrogen-filled nano-sized pores that pinned the grain boundaries. Our study reveals that a combination of severe shear strain and surface attrition causes the capture of N_2 molecules in the near-surface layer of the deformed metal from the ambient atmosphere. This phenomenon may play an important role in formation of percolating porosity in metals processed by severe plastic deformation.

© 2019 Acta Materialia Inc. Published by Elsevier Ltd. All rights reserved.

Poor thermal stability is a critical issue in ultrafine-grained and nanostructured crystalline materials, and one of the reasons hindering their applications [1–3]. High thermal stability means low grain boundary (GB) migration rate and limited grain coarsening at elevated temperatures [4]. This can be achieved by reducing the energy and intrinsic mobility of the GBs or by introducing objects dragging the GB migration, such as impurity atoms, precipitates or pores [5,6]. It is worth noting that in this letter we consider only general high-angle GBs. Low-angle and special GBs are not considered as they have low energy and account for a minor fraction of the GBs in polycrystalline materials [7].

Alloying with a second component is a straightforward way to increase the thermal stability of nanocrystalline materials. There are two reasons for the stabilization of the microstructure by alloying: Firstly, the segregation of alloying elements at the GBs lowers their energy and reduces the thermodynamic driving force of grain growth [8–10]. Secondly, solute atoms segregating at the GBs reduce their mobility due to the solute drag effect [11]. In both cases, alloying pure metal with the components segregating at the GBs is essential [12–14]. However, a recent study by Zhou et al. demonstrated a marked thermal stability of the nano-grains in top 20 μm-thick surface layer in the Cu rod of a 99.97 wt% purity processed by surface mechanical grinding in liquid nitrogen [15]. They attributed this stabilization of nanoscale microstructure to the relaxation of GBs and reduction of their energy during the *in-situ* plastic straining and dynamic recrystallization [15].

In the present study we uncovered extraordinarily high thermal stability of ultrafine-grained (UFG) surface layers of Cu processed by high-pressure torsion (HPT). We used a 99.9995 wt% (5N5) purity Cu disk as the model material to exclude any alloying effects. The Cu disk was processed by HPT at room temperature. The HPT processing (5 anvil rotations at a rotation rate of 1 revolution per minute) was carried out under compressive pressure of 5 GPa in a Bridgman anvil-type unit with a quasi-constrained die using a custom-built computer-controlled device. We prepared the cross-sectional samples and characterized the UFGs regions of the Cu disk employing scanning electron microscopy (SEM) and scanning transmission electron microscopy (STEM) in bright-field (BF) and high-angle annular dark-field (HAADF) modes (see Supplementary Material).

The 5 μm thick surface layer of the as-processed Cu disk exhibits gradient microstructure (Fig. 1a). The shape of the UFGs changes from elongated (average width of 26 ± 9 nm and length

* Corresponding authors.
E-mail addresses: yuanshen.qi@campus.technion.ac.il (Y. Qi), ann7606@yandex.ua (A. Kosinova), askar.kilmametov@kit.edu (A.R. Kilmametov), straumal@issp.ac.ru (B.B. Straumal), erabkin@technion.ac.il (E. Rabkin).

https://doi.org/10.1016/j.scriptamat.2019.10.050
1359-6462/© 2019 Acta Materialia Inc. Published by Elsevier Ltd. All rights reserved.

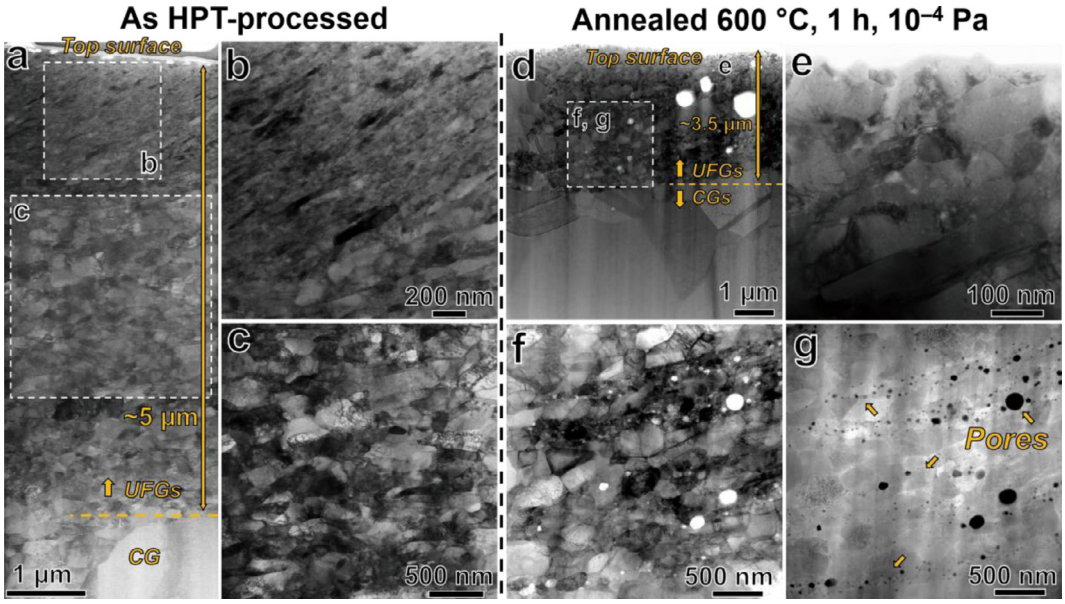

Fig. 1. The surface layer of ultrafine grains in the HPT-processed 5N5 purity Cu exhibits high thermal stability. (a–c) BF-STEM characterization of the ~5 µm thick surface layer with the UFGs and a gradient microstructure in the as-processed Cu disk; (b, c) are enlarged views of the inserts in (a). (d–g) STEM characterization of the UFGs in the surface layer after annealing at 600 °C; (e–g) are enlarged views of the inserts in (d); (e) is from the top edge region in (d); (f) and (g) are the BF- and HAADF-STEM micrographs from the same region and highlight the co-existence of UFGs and pores.

of 141 ± 93 nm) to equiaxed one (average diameter of 208 ± 78 nm) with increasing depth, as seen in Fig. 1 (b and c). Farther away from the top surface towards the disk interior, coarse grains (average size of ~5 µm) were observed (Fig. S1). These coarse grains (CGs) formed due to recrystallization and coarsening at ambient temperature during storage, which is often observed in high purity Cu processed by severe plastic deformation (SPD) [16,17], and was also reported in our previous study (see Supplementary material) [18]. The UFGs in the top 5 µm-thick surface layer did not exhibit any growth, even after low-temperature annealing (120 °C, 20 min) [18].

The high thermal stability of the UFGs in the top surface layer was further verified by heat treatment at elevated temperatures. After annealing of the HPT-processed Cu disk at 600 °C (0.64 T_m, where T_m is the melting temperature of Cu) for 1 h in an evacuated quartz ampoule (residual pressure 10^{-4} Pa), the UFGs in the top ~3.5 µm surface layer experienced only a moderate growth (Fig. 1d). Closer inspection reveals that the average grain size in the UFG layer increased from 100 ± 70 nm (Fig. 1e) to 265 ± 132 nm (Fig. 1f). Moreover, we observed high density of spherical pores with diameters ranging from 10 to 173 nm in the UFG region of the annealed sample (see Fig. 1g). These pores probably played a key role in stabilization of the UFG microstructure, since no pores were observed in the adjacent CG region (see Fig. 1d).

We would like to emphasize that the high thermal stability of UFGs in the top ~3.5 µm layer is an extraordinary phenomenon, because there were no alloying elements to segregate at the GBs or to impede the GB migration via the solute drag. Also, the grain size is in the submicrometer range (100–300 nm), which is above the critical nanoscale grain size (43 ± 2 nm) for the GB relaxation [15].

To verify the contribution of the pores (seen in Fig. 1g) to the GB drag and stabilization of the UFGs, one and the same region of the sample should be observed before and after heat treatment. To this end, we performed quasi-in-situ heat treatments on a lift-out lamella to track the UFG microstructure of the top surface layer. The lift-out process of the 3 µm thick lamella was performed in a focused ion beam (FIB) – SEM dual beam microscope. This relatively high thickness of the TEM lamella ensured the quasi-3D nature of grain growth and minimized the effect of free surfaces and surface diffusion. The annealing was conducted in a rapid thermal annealing furnace under residual pressure of 5 Pa (see Supplementary materials). In the as-processed sample, the UFG layer in the top surface and CGs with annealing twins are clearly seen in Fig. 2a. No pores in the UFG layer could be distinguished in the SEM image acquired with higher magnification (Fig. 2b). Annealing at 200 °C for 20 min resulted in an expansion of the CG region (Fig. 2c), yet a part of the UFG layer close to the surface was preserved and pores appeared within it (Fig. 2d). STEM characterization of the same lamella after additional FIB thinning to the thickness of about 100 nm revealed that the UFG layer was ~1.5 µm thick and the diameter of the nano-pores ranged from 5 to 50 nm, as can be seen in Fig. 2 (e–g). This indicates that the high thermal stability of UFGs in the top surface layer was related to the existence of the pores. It is worthwhile to note that very high thermal stability has been observed in nanocrystalline Cu thin films produced by ion beam assisted deposition, and was also associated with the presence of nanometer-sized voids [19]. It was concluded that the voids were formed by the agglomeration of excess vacancies induced by Ar ion beam bombardment during sample preparation [19].

In the present work, the formation and growth of pores during annealing raised two questions – how these pores formed and why they did not shrink during annealing. To study the origin of the pores, we performed a high resolution HAADF - STEM study of the UFGs in the top surface layer of the as-processed sample. As seen in Fig. 3(a and b), the top UFG layer exhibits high density of homogeneously distributed nano-pores (with the radius of 3–6 nm). These nano-pores in the as-processed sample were not visible in SEM and low magnification STEM, yet they increased in size during annealing and became visible (Fig. 1d). Energy-dispersive X-ray spectroscopy (EDX) mapping did not reveal any oxygen segregation in the pores (Fig. 3e). Assuming that the pores in the as-processed sample are empty raises the question how did they survive the high temperature heat treatment, which normally causes the pores to shrink, collapse and disappear [20]. The upper bound for the time of pore shrinkage, τ, can be determined assuming vacancy-mediated bulk diffusion [21]. We employed the relationship

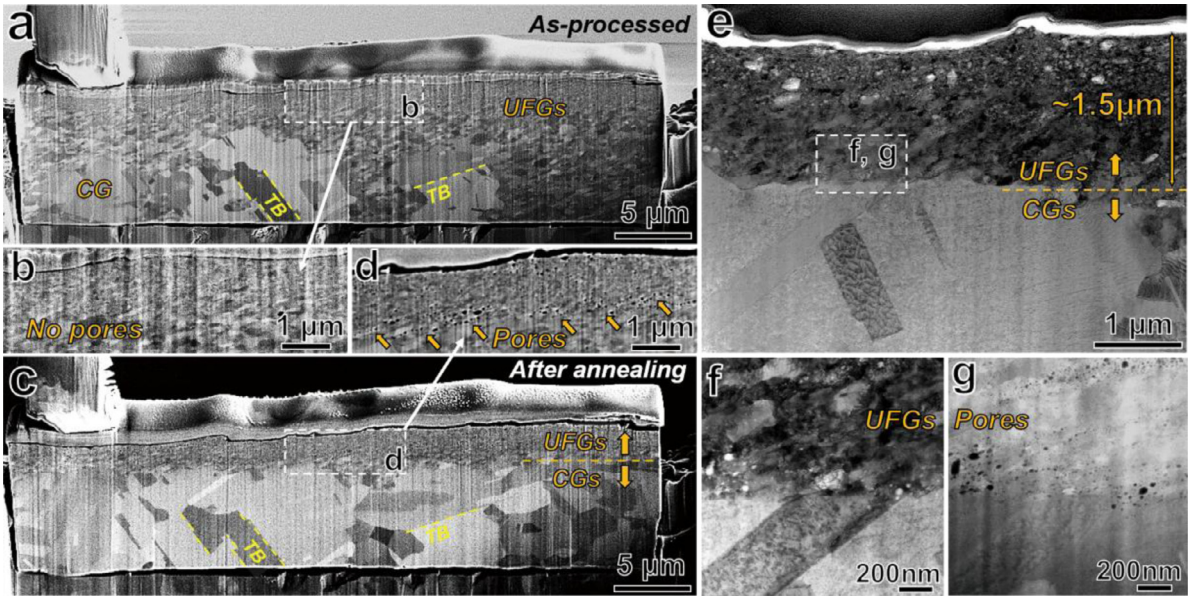

Fig. 2. The co-existence of UFGs and pores in the top surface layer verified by quasi-in-situ characterization. (a, b) SEM images of the lamella lifted out from the as-processed Cu disk, which exhibit clear UFGs in the top surface region and some CGs with annealing twins beneath it; (b) is the higher magnification micrograph of the top surface UFG layer in which no pores could be observed. (c, d) SEM images of the same lamella after annealing at 200 °C for 20 min; the ~1.5 μm thick UFG layer can still be observed in the near-surface region; (d) is the higher magnification micrograph of the top surface UFG layer exhibiting high density of pores. (e) BF-STEM imaging of the UFG layer after annealing and thinning of the TEM lamella; (f. g) are the BF- and HAADF-STEM micrographs from the same region and highlight the co-existence of UFGs and pores. Note the twin boundaries (TBs) in (a, c), which indicate that the same lamella was examined before and after annealing.

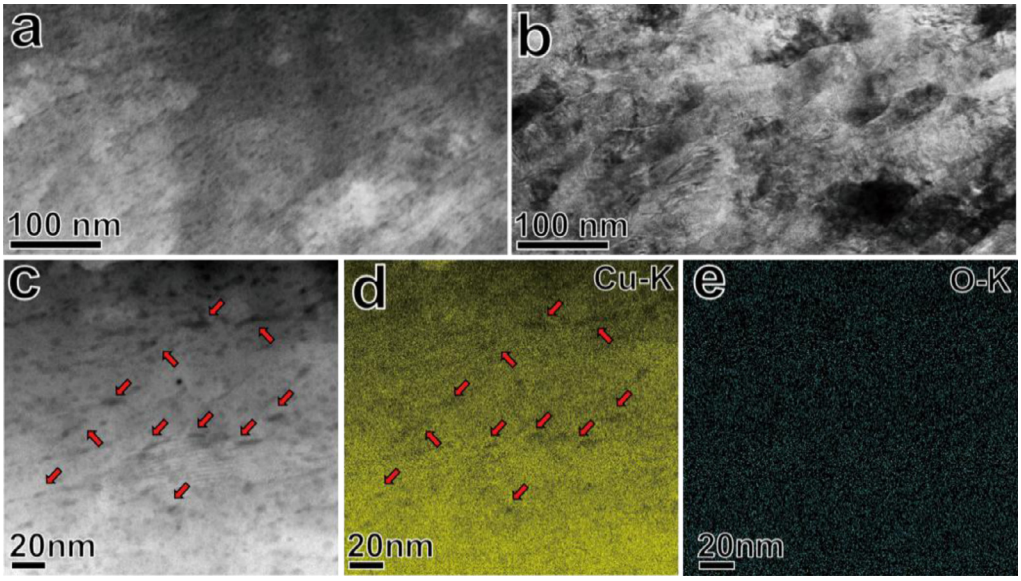

Fig. 3. Nano-pores in the top surface layer of the as-processed sample. (a, b) HAADF- and BF-STEM images showing the uniform distribution of nano-pores in the top UFG surface layer. (c–e) EDX characterization confirmed the existence of nano-pores and excluded oxygen enrichment in them.

proposed by Westmacott et al. [22]:

$$\tau = \frac{kT}{6D_V\gamma_S\Omega}\cdot R_0^3, \quad (1)$$

where R_0 (10 nm, upper estimate) is the initial pore radius, γ_S=1.46 J/m^2 is the weighted surface energy of Cu [23], and Ω=1.2·10^{-29} m^3 /at is the atomic volume of Cu. D_V is the bulk self-diffusion coefficient of Cu which can be estimated from the following Arrhenius relationship

$$D_V(T) = D_V^0 \exp\left(-\frac{Q}{kT}\right). \quad (2)$$

where D_V^0 ≈0.2·10^{-4} m^2 s^{-1} and Q≈ 197.2 kJ mol^{-1} are the pre-exponential factor and activation enthalpy of diffusion, respectively [24]. At the annealing temperature employed in the present study (T=873 K), D_V≈2.1·10^{-17} m^2/s. With this diffusivity, Eq. (1) yields the shrinkage time of 6 s. The true shrinkage time should be significantly shorter due to the contribution of the GB diffusion which was not accounted for in Eq. (1). Based on this estimate, we conclude that there should be some physical factor preventing the pore shrinkage.

One such factor could be gas trapped within the pores, similar to the phenomenon of irradiation-induced swelling of metals [25,26]. During the HPT treatment in the ambient atmosphere, some air or its constituents could be trapped in the near-surface region of the processed sample. Since the EDX measurements did not detect any oxygen in the pores, another candidate could be

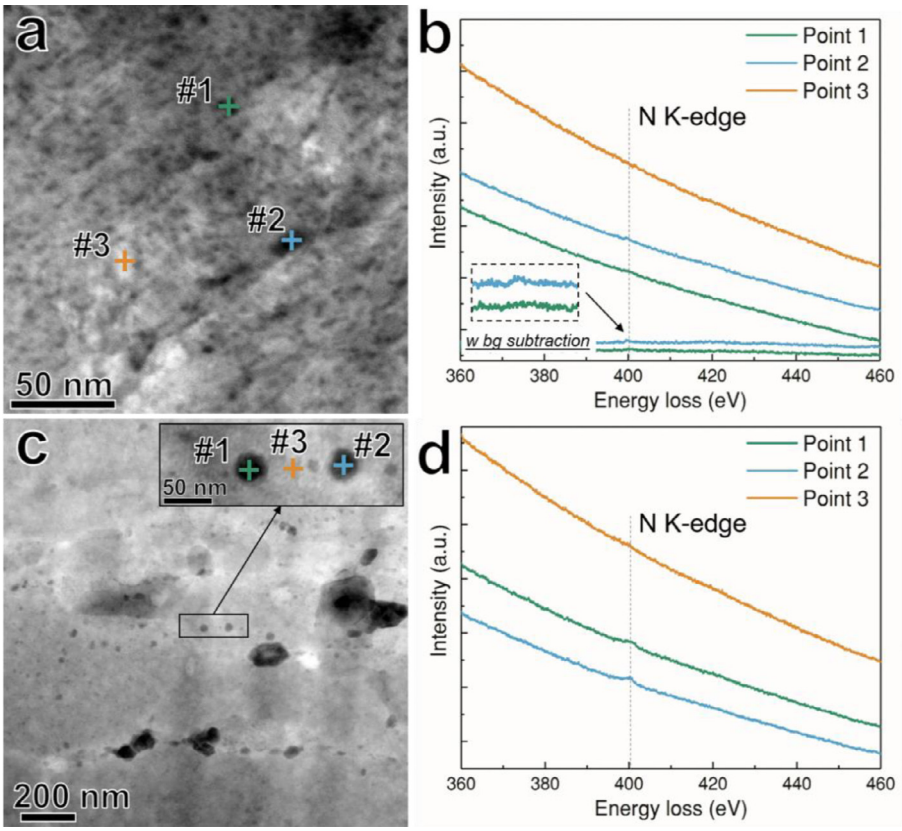

Fig. 4. EELS characterization revealing nitrogen in the nano-pores in the as-processed and annealed samples. (a, b) show the annular dark-field (ADF) image of the nano-pores in as-processed sample and EELS spectra from three locations. (c, d) show the ADF image of the nano-pores in the sample annealed at 600 °C for 1 h under the vacuum of 10^{-4} Pa and EELS spectra from three locations. In both samples, points 1 and 2 correspond to the pores exhibiting dark contrast in the ADF images. Point 3 is located in the pore-free Cu region. (b) contains two spectra with background (w bg) subtraction for highlighting the N K-edge peak.

nitrogen. Because the K-edge of N (at around 401 eV) can hardly be distinguished in the EDX spectrum, we used electron energy loss spectroscopy (EELS) to analyse the chemical composition of the pores. As can be seen in Fig. 4, clear nitrogen K-edge at ~401 eV was observed during local analysis of the nano-pores. This result proved the presence of N_2 in the nano-pores. Comparing to Fig. 4d (the sample annealed at 600 °C for 1 h under the vacuum of 10^{-4} Pa), the N K-edge in as-processed sample (Fig. 4b) is less obvious due to smaller pore sizes and small amount of N_2 in the pores. It should be noted that we performed EELS point analysis of 25 pores in the annealed sample, but only found clear N-edge in three pores. This means that during FIB milling, some pores were opened causing the N_2 gas leakage. We believe that nitrogen, rather than oxygen was detected within the pores because of its higher concentration in the ambient air, and much lower solubility in the solid Cu [27-30].

We estimated the volume fraction of N_2 –filled nano-pores in the Cu surface layer of the as-processed sample based on Fig. 4(a). The nano-pores were assumed to have spherical shape and their total volume was calculated to be ~1050 nm^3. The thickness of the Cu in this region was estimated using EELS-based log-ratio technique [31]. The mean number of scattering events per incident electron obtained from the low-loss spectrum, t/λ, was 1.7–1.9; and the estimated average thickness of the measured area was ~150 nm. The volume fraction of N_2-filled nano-pores was estimated as ~0.1%.

We believe that nitrogen penetrated into Cu during the HPT processing in molecular, rather than atomic form. This is because high pressure (>50 GPa) and temperatures (>1500 K) are required for breaking the N–N bonds and forming the Cu-N bonds [32]. Some molecular oxygen could also be trapped in Cu during processing, but since it exhibits much higher solubility in Cu than nitrogen it can be readily dissolved in the matrix during annealing [30,33].

There are two possible penetration routes of molecular nitrogen into Cu during HPT processing. Firstly, the GBs and triple junctions formed during HPT exhibit anomalously high diffusivity and free volume [10,34], so that they probably can conduct molecular nitrogen. Secondly, plastic instability induced by friction deformation (relative slippage and sliding between Cu disk and HPT anvil) on the Cu surfaces is another reason for the capture of molecular N_2. Some micro- or nano-cracks on the surface cannot be avoided [35–37]; and they can capture and enclose the N_2 molecules during deformation. Moreover, the intrinsic instabilities of turbulent plastic flow during HPT can also cause the N_2 capture [38,39]. Once inside the pores, nitrogen prevents their shrinkage at high temperatures, since the increasing gas pressure counterbalances the capillary pressure which is the driving force for pore shrinkage. The equilibrium vacancy concentration near the pores with higher quantities of the trapped N_2 and higher internal gas pressure becomes lower than the average concentration in the sample, causing these pores to grow at the expense of their counterparts containing less N_2. This coarsening-like process results in decreasing number and increasing average size of the pores during annealing. These pores pin the GBs and slow down their migration, thus preserving the UFG microstructure in the pores-containing regions.

An important role of the trapped gases in preserving of internal porosity in metals uncovered in the present work sheds a new light on persistence of ultrafast diffusivity paths after annealing of metals processed by severe plastic deformation [40–42]. Indeed, the elongated gas-filled pores at the triple junctions may stabilize the UFG microstructure and ensure the existence of continuous

percolating diffusion paths along the internal surfaces of the pores even after annealing at relatively high homological temperatures. High internal gas pressure in such pores should prevent their shrinkage at elevated temperatures.

In conclusion, we uncovered the phenomenon of capture of N_2 molecules from the ambient atmosphere in severely deformed metals, which was overlooked in the previous studies. The combination of hydrostatic pressure, shear strain and friction deformation contribute to the formation of ~0.1 vol% of nano-pores (of ~10 nm in diameter) in the top ~5 μm surface layer of the disk of ultrahigh purity Cu processed by high-pressure torsion. These nano-pores pinned the GBs and slowed down their migration, contributing to a very high thermal stability (up to 1 h at 600 °C) of the UFG microstructure. Thus, designing the nano-pores filled with different gases can be employed as a tool for improving the thermal stability of ultrafine-grained and nanostructured metallic materials.

Declaration of Competing Interest

None.

Acknowledgments

The technical assistance and helpful advices of Dr. Yaron Kauffmann and Dr. Larisa Popilevsky are heartily acknowledged. The work was supported by the Ministry of Science & Technology, Israel (grant 3-12418), and by Russian Foundation for Basic Research (grant 15-53-06008). YQ would like to thank the support by Technion-Guangdong Postdoctoral Fellowship.

Supplementary material

Supplementary material associated with this article can be found, in the online version, at doi:10.1016/j.scriptamat.2019.10.050.

References

[1] Y. Estrin, A. Vinogradov, Acta Mater. 61 (2013) 782–817.
[2] J. Weissmüller, Nanostruct. Mater. 3 (1993) 261–272.
[3] T. Chookajorn, H.A. Murdoch, C.A. Schuh, Science 337 (2012) 951–954.
[4] F.J. Humphreys, M. Hatherly, Recrystallization and Related Annealing Phenomena, 2nd ed., Elsevier, 2012.
[5] G. Gottstein, L.S. Shvindlerman, Grain Boundary Migration in Metals: Thermodynamics, Kinetics, Applications, 2nd ed., CRC Press, 2009.
[6] R.A. Andrievski, J. Mater. Sci. 49 (2014) 1449–1460.
[7] W. Cai, W.D. Nix, Imperfections in Crystalline Solids, 1st ed., Cambridge University Press, 2016.
[8] E. Ruckenstein, Chem. Phys. Lett. 57 (1978) 517–521.
[9] A.R. Kalidindi, T. Chookajorn, C.A. Schuh, JOM 67 (2015) 2834–2843.
[10] Y. Amouyal, S. Divinski, Y. Estrin, E. Rabkin, Acta Mater. 55 (2007) 5968–5979.
[11] J.W. Cahn, Acta Metall. 10 (1962) 789–798.
[12] H.A. Murdoch, C.A. Schuh, Acta Mater. 61 (2013) 2121–2132.
[13] K. Darling, M. Tschopp, B. VanLeeuwen, M. Atwater, Z. Liu, Comput. Mater. Sci. 84 (2014) 255–266.
[14] D. Amram, C.A. Schuh, Acta Mater. 144 (2018) 447–458.
[15] X. Zhou, X. Li, K. Lu, Science 360 (2018) 526–530.
[16] Y. Huang, S. Sabbaghianrad, A.I. Almazrouee, K.J. Al-Fadhalah, S.N. Alhajeri, T.G. Langdon, Mater. Sci. Eng. A 656 (2016) 55–66.
[17] Y.L. Wang, R. Lapovok, J.T. Wang, Y.S. Qi, Y. Estrin, Mater. Sci. Eng. A 628 (2015) 21–29.
[18] Y. Qi, A. Kosinova, A.R. Kilmametov, B.B. Straumal, E. Rabkin, Mater. Charact. 145 (2018) 1–9.
[19] H. Ma, Y. Zou, A.S. Sologubenko, R. Spolenak, Acta Mater. 98 (2015) 17–28.
[20] Z. Zhang, T. Liu, A.E. Smith, N.V. Medhekar, P.N. Nakashima, L. Bourgeois, J. Appl. Crystallogr. 49 (2016) 1459–1470.
[21] T. Volin, R. Balluffi, Phys. Status Solidi B 25 (1968) 163–173.
[22] K. Westmacott, R. Smallman, P. Dobson, Metal. Sci. J. 2 (1968) 177–181.
[23] K.C. Mills, Y. Su, Int. Mater. Rev. 51 (2006) 329–351.
[24] A. Kuper, H. Letaw Jr, L. Slifkin, E. Sonder, C. Tomizuka, Phys. Rev. 98 (1955) 1870.
[25] L.K. Mansur, Nucl. Technol. 40 (1978) 5–34.
[26] S.H. Li, J.T. Li, W.Z. Han, Materials 12 (2019) 1036.
[27] M. Hansen, K. Anderko, Constitution of Binary Alloys, 2nd ed., McGraw-Hill Companies, Inc., New York, 1958.
[28] J. Davis, ASM International Handbooks: Copper and Copper Alloys, ASM International, Materials Park, 2001.
[29] A.M.M. Noor, N.H.M. Nor, S. Yokoyama, High Temp. Mater. Process. 36 (2017) 1035–1038.
[30] V.M. Horrigan, Metall. Trans. A 8 (1977) 785–787.
[31] T. Malis, S. Cheng, R. Egerton, J. Electron Microsc. Tech. 8 (1988) 193–200.
[32] J. Binns, M.E. Donnelly, M. Peña-Alvarez, M. Wang, E. Gregoryanz, A. Hermann, P. Dalladay-Simpson, R.T. Howie, J. Phys. Chem. Lett. 10 (2019) 1109–1114.
[33] Z. Liu, C. Patzig, S. Selle, T. Höche, P. Gumbsch, C. Greiner, Scr. Mater. 153 (2018) 114–117.
[34] B. Oberdorfer, D. Setman, E.-.M. Steyskal, A. Hohenwarter, W. Sprengel, M. Zehetbauer, R. Pippan, R. Würschum, Acta Mater. 68 (2014) 189–195.
[35] J. Ribbe, G. Schmitz, H. Rösner, R. Lapovok, Y. Estrin, G. Wilde, S.V. Divinski, Scr. Mater. 68 (2013) 925–928.
[36] L. Meshi, S. Samuha, S.R. Cohen, A. Laikhtman, A. Moshkovich, V. Perfilyev, I. Lapsker, L. Rapoport, Acta Mater. 59 (2011) 342–348.
[37] I. Popov, A. Moshkovich, S.R. Cohen, V. Perfilyev, A. Vakahy, L. Rapoport, Wear 404-405 (2018) 62–70.
[38] Y. Qi, A. Kosinova, A.R. Kilmametov, B.B. Straumal, E. Rabkin, Mater. Charact. 145 (2018) 389–401.
[39] M. Pouryazdan, B.J. Kaus, A. Rack, A. Ershov, H. Hahn, Nat. Commun. 8 (2017) 1611.
[40] J. Ribbe, D. Baither, G. Schmitz, S.V. Divinski, Phys. Rev. Lett. 102 (2009) 165501.
[41] S. Divinski, G. Wilde, E. Rabkin, Y. Estrin, Adv. Eng. Mater. 12 (2010) 779–785.
[42] D. Prokoshkina, L. Klinger, A. Moros, G. Wilde, E. Rabkin, S.V. Divinski, Scr. Mater. 101 (2015) 91–94.